WIDE DYNAMIC RANGE FIBER-OPTIC ALIGNMENT TRANSFER DEVICE

Leonard S. Wilk
Robert P. Dahlgren

The Charles Stark Draper Laboratory, Inc.
555 Technology Square
Cambridge, Massachusetts 02139

ABSTRACT

An interferometric fiber-optic bending strain sensor measuring deflections (angular and displacement) between reference points is described. This sensor has many applications in architecture, geology, inertial referencing, navigation instrumentation, and towed-array shape sensing. The sensor consists of a set of modified Mach-Zehnder interferometers, mounted on a flexible member. By judicious choice of interferometer arrangement, bending moments in several orthogonal degrees of freedom can be extracted. A wide dynamic range readout technique is used to measure deflection in a bidirectional, absolute sense. A simple algorithm converts the interferometer output, which is a function of bending strain, to spatial coordinate corrections for the two ends of the flexible member.

INTRODUCTION

In several fields there is a need to continually measure the spatial and angular alignment between two or more objects. Civil engineering, geology, inertial navigation and its testing, metrology underwater towed array instrumentation, smart structures, and avionics integration are just a few of the many application areas. To be useful in the real world, an alignment characterization system must have high accuracy and resolution and must be able to withstand severe environmental and operational insults.

Fiber-optic strain gauges can be made by using a pair of single-mode fibers operated differentially and forming a Young's interferometer [1]. Such strain gauges absolute change of length (i.e., ΔL = number of fringes = output) while

common resistive strain gauges measure relative changes of length (i.e., $\Delta L/L = \Delta R/R$ = output). Consequently, fiber-optic strain gauges become more sensitive (in measuring integrated strain) as the length scale of the application increases, compared to most other types of strain gauges. The gauges are also distributed transducers so one can use techniques such as winding or bonding the fibers in particular patterns to vary a given transducer's spatial characteristics.

ALIGNMENT TRANSFER BY INTEGRATED STRAIN (AXIS)

Instrumenting a flexible cable with fiber optics to measure positional deviations is based on attaching optical fiber pairs on the cable section and measuring their length difference by interferometric methods [2]. The three rotation angles of one end with respect to the other will be directly related to the length differences measured by three fiber pairs and the cable's diameter. This is shown in Figure 1, where two rotations (Θ_y and Θ_p) are measured with two optical fiber pairs bonded longitudinally along the cable and where cable twist (Θ_r) is measured with an optical fiber pair counter-wound helically along the cable.

$$\Theta_y = \frac{(+x) - (-x)}{D}$$

$$\Theta_p = \frac{(+y) - (-y)}{D}$$

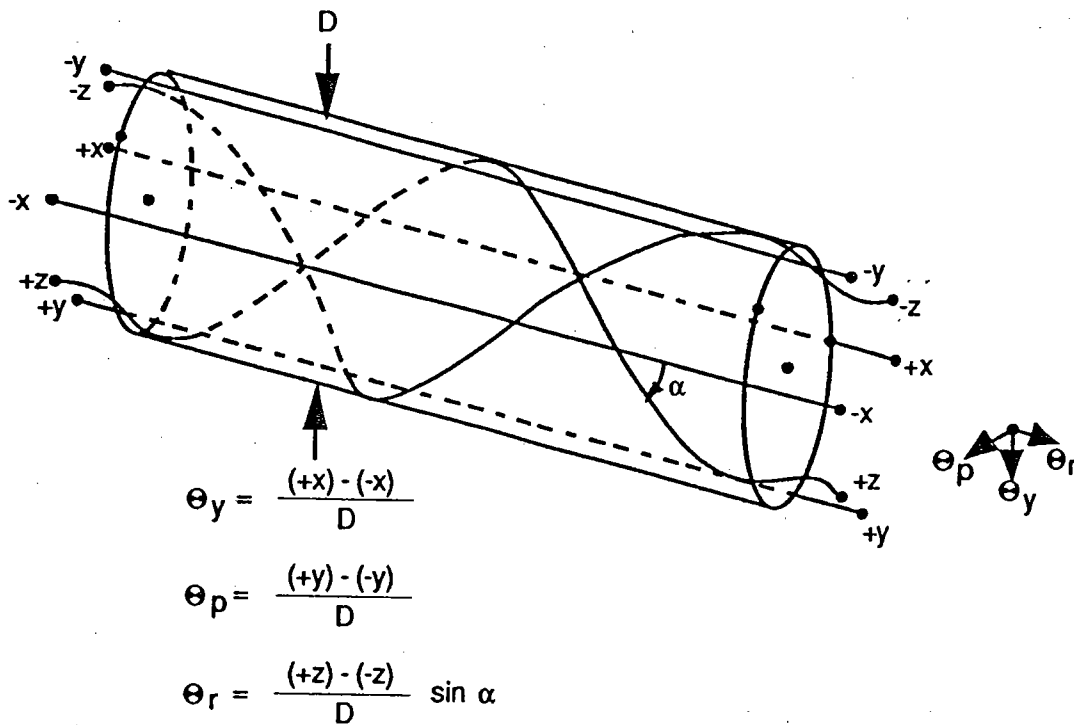$$\Theta_r = \frac{(+z) - (-z)}{D} \sin \alpha$$

Figure 1. Three-axis AXIS arrangement.

An analysis was undertaken to develop the equations for the general case of translating integrated strain on a flexible cable to angular rotations and deflections for the single-axis case, as shown in Figure 2. The output ϵ of an integrating strain sensor (i.e., an output that is proportional to the change in length of the sensor that extends from point 0 to point L) is given by

$$\Delta L \equiv \epsilon = \int_0^L p(x)\, b(x)\, w''(x)\, dx$$

(1)

where the sensor has a variable sensitivity, or weighting, as a function of position $p(x)$. The sensor is displaced from the cable's centerline by $b(x)$ and has a displacement of $w(x)$ from the x-axis.
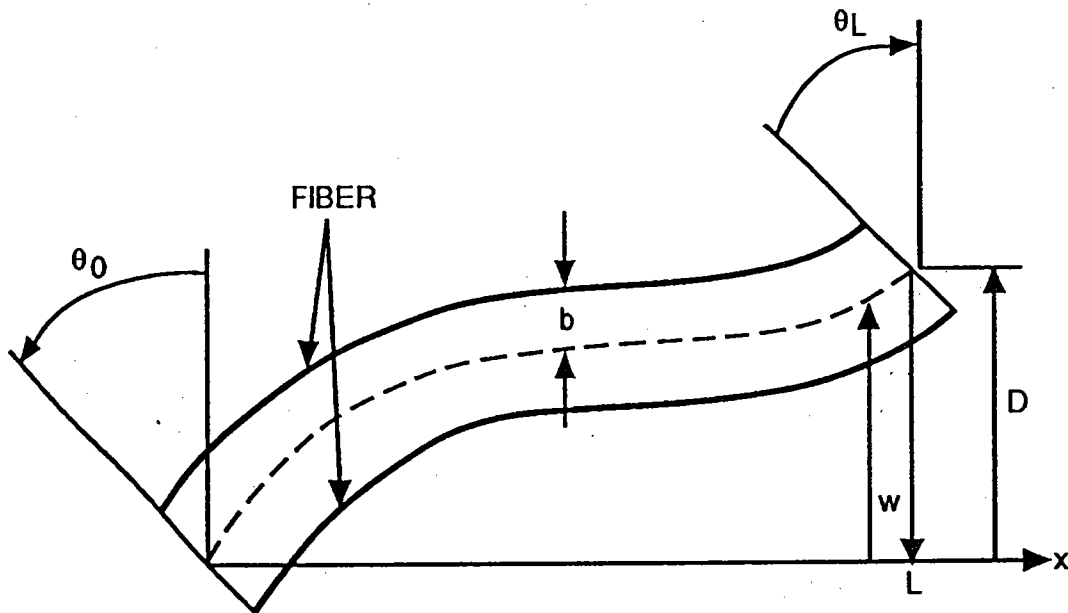

Figure 2. Single-axis case.

If the sensor is displaced from the neutral axis of the cable by a constant value, i.e., $b(x) = B$, then the integrating strain sensor's output will be:

$$\epsilon = p(x) B w'(x)\Big|_0^L - p'(x) B w(x)\Big|_0^L + \int_0^L p''(x) B w(x) dx \tag{2}$$

Further, if the weighting function of the sensor is uniform along the length, i.e., $p(x) = P$, then the output of the integrating strain sensor will be:

$$\epsilon = PB (w'(L) - w'(0)) = PB (\theta_L - \theta_0) \tag{3}$$

In other words, this analysis shows that the output will be proportional to the angular differences between the ends, *regardless of the cable's length and shape.* (A more detailed analysis places constraints on this attribute. These constraints require that the cable deformation stays in the elastic region and that radii of curvature remain large compared to the diameter of the cable.)

If the strain sensor has proportional weighting (i.e., the sensitivity diminishes uniformly from the left end to the right end, i.e., $p = K(1 - x/L)$, then the integrating strain sensor's output will be linearly related to the angle and the deflection D, regardless of the shape of the cable:

$$\epsilon = -KB w'(0) + \frac{KB}{L} (w(L) - w(0)) = -KB(\theta_0 + D/L) \tag{4}$$

Thus, we see that angle and displacement of two reference points can be measured by integrating strain sensors. In the case of an optical fiber, the optical phase shift as a function of strain is given by the photoelastic effect

$$\phi(\epsilon) = knL(1 + \epsilon) - \frac{kn^3L}{2}\left(\rho_{12} - \nu(\rho_{11} + \rho_{12})\right)\epsilon \tag{5}$$

where $k = 2\pi/\lambda$, n is the refractive index, ν is Poisson's ratio, and ρ_{11} and ρ_{12} are the photoelastic constants. The cable would be instrumented with pairs of integrating strain sensors on opposite sides of the cable, operating in a differential mode.

Solid-State Optical Materials

INTERFEROMETER DESIGN

An interferometric fiber-optic strain gauge sensor was chosen because of wide dynamic range, wide bandwidth, flexibility of winding configurations, and inherent differential operation. The design chosen was a modified Young's interferometer, built using optical fiber in lieu of pinholes. This technique was successfully used to evaluate γ-radiation effects on the refractive index of optical fiber [3]. Refer to Figure 3. Light from a narrow linewidth laser is split by a 50/50 coupler, with the two arms forming the differential strain sensors. The expression for the free-space optical irradiance distribution exiting the mth fiber is roughly

$$I_m(x,y) = \frac{2P_m}{\pi w^2} e^{-2x^2/w^2} e^{-2y^2/w^2} \qquad m = 1,2 \tag{6}$$

P_m is the total power guided in fiber m. The parameter w is the beam waist radius, defined as the point where intensity drops to $1/e^2$ (electric field drops by $1/e$). Far from the fiber endfaces, w is approximated by

$$2w \approx \Theta l \qquad \text{local beam waist}$$

$$\Theta/2 = \sin (\text{N.A.}) \qquad \text{fiber acceptance half-angle}$$

$$\text{N.A.} = \sqrt{n_{core}^2 - n_{clad}^2} \qquad \text{fiber numerical aperture}$$
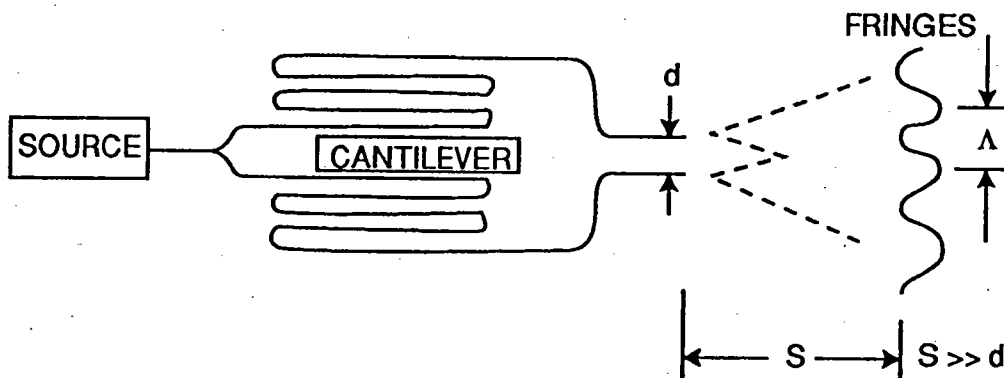

Figure 3. Interferometer schematic.

The two polished fiber endfaces are brought into close proximity such that the pair of exiting Gaussian beams overlap in space. In the overlap region far from the fibers, the two spherical waves interfere to provide a fringe pattern in that three-dimensional space. This fringe pattern will consist of alternating bright and dark regions. If the fringe pattern is observed at a plane perpendicular to the fibers, the fringes will be straight and parallel to another. The fringe pattern's position is a linear function of the relative phase of the two interferometer arms. If the fringe pattern is observed at a plane perpendicular to the fibers at a large distance s, the fringe spatial frequency Λ is approximately by [4]

$$\Lambda \approx \lambda s / d \qquad s \gg d \tag{7}$$

where d is the separation of the fiber cores at the endfaces (at $z = 0$) and λ is the operating wavelength. It should be noted that to get reasonably large fringe spacing, the cores of the fibers at the endfaces must be very close (10-20 microns) for a compact design. Assuming perfect beam overlap requires the two fiber cores to match, be parallel, and be separated by a small distance. The resultant fringe pattern will be along the x-axis, which is defined as being parallel to a line separating the fiber cores. The optical intensity at a distance $z = s$ from the fiber endfaces is calculated to be

$$I_m(x,y) = \frac{4P_0}{\pi w^2} e^{-2x^2/w^2} e^{-2y^2/w^2} \left(1 + \eta \cos\left(\frac{\pi x}{\Lambda} + \frac{\phi}{2} \right) \right) \tag{8}$$

where w is the beam waist, which can be approximated by $w \approx \Theta l / 2$. ϕ is the relative phase shift between the two interferometer arms. P_0 is the total optical power guided in the fibers $= P_1 + P_2$. The two exponential terms describe the circular Gaussian beam profile, and the cosine term is the fringes. The factor η is the fringe visibility or contrast, defined as

$$\eta = \frac{I_{max} - I_{min}}{I_{max} + I_{min}} \tag{9}$$

Solid-State Optical Materials

Contrast is a function of the power level mismatch in the two fiber legs, optical source coherence, path length mismatch, and polarization misalignment. For the case of 100-percent contrast, i.e., $P_1 = P_2$, the polarization states are aligned, adequate coherence exists, η is equal to unity, and the above equation reduces to

$$I_m(x,y) = \frac{4P_0}{\pi w^2}\, e^{-2x^2/w^2}\; e^{-2y^2/w^2}\; \cos^2\!\left(\frac{\pi y}{\Lambda} + \frac{\phi}{2}\right)$$

(10)

Constructing the optical part of the experiment is straightforward, due to Draper's ongoing optical fiber component development. In order to get a large fringe spacing, part of the 125-μm diameter cladding must be removed to bring the cores into close proximity. This can be accomplished by bonding the fiber into a glass block with a suitable groove in it, as shown in Figure 4. This provides mechanical support for cladding removal, which is done by grinding and polishing. If the fiber was birefringent, the block's flat surface can be used to align the fiber's principal axes. Care must be taken not to polish into the cladding too far which would allow optical coupling between the cores. Also, care must be taken to get a scatter-free, right-angle fiber endface surface. Once the lapping and polishing operation is completed, two such prepared fibers are placed into an alignment fixture. This allows stable adjustment of the fiber core separation to obtain optimum fringe spacing. The interferometer's design permits some of the random phase drift caused by temperature, vibration, etc., to be common-mode rejected. This fringe-generation technique has been demonstrated to yield stable, high-contrast fringes.
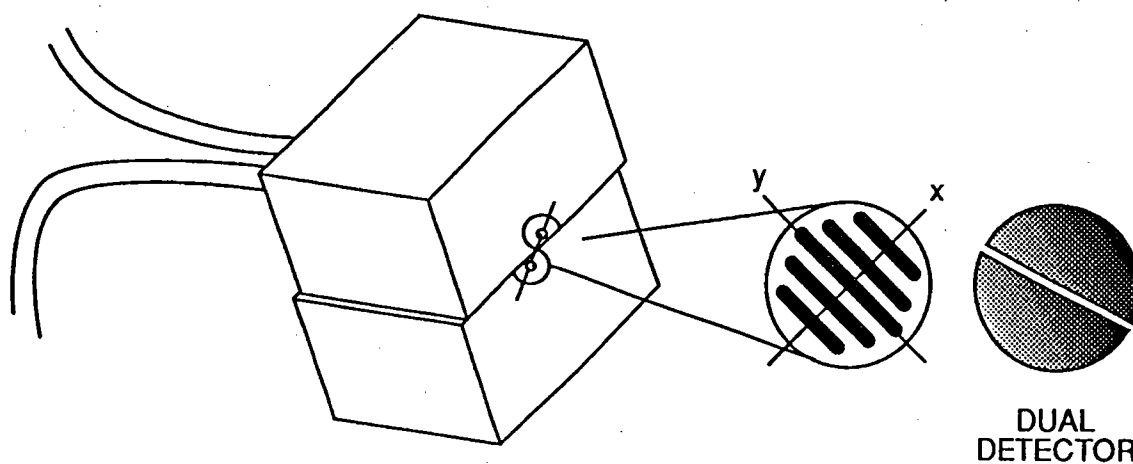

Figure 4. SQD readout.

There are several approaches to extracting wide dynamic range, high-resolution, open-loop phase information from interferometers [5, 6, 7]. This general technique is often called homodyne demodulation; the exact approach used depends on bandwidth considerations, and other tradeoffs. In our approach, a quadrature-type output is generated from the fringe pattern, which is a sinusoid and cosinusoid signal. This Spatial Quadrature Demodulation (SQD) technique allows wide dynamic range while having good sensitivity and frequency response.

A pair of photodetectors, having a precise gap defined between them, is illuminated by the fringe pattern. To calculate the power on a detector pair, one evaluates

$$\iint\limits_{\text{det } 1} I(x,y) \, \partial x \partial y \quad \text{and} \quad \iint\limits_{\text{det } 2} I(x,y) \, \partial x \partial y \tag{11}$$

If the fringe spacing Λ is adjusted such that it is 4× the detector gap width, the two detectors will detect a signal proportional to $\sin\phi$ and $\cos\phi$ plus a dc component. This signal is conditioned by a transimpedance amplifier, offset, and gain matching circuitry (see Figure 5). A low-pass filter, which is not shown, may be employed to minimize $\sqrt{BW}$ noise. The fringe spacing is adjusted to meet the quadrature condition by adjusting fiber endface spacing. Due to the alignment system's geometry, the detector pair must be rotated such that the gap remains parallel to the fringes. An oscilloscope lissajous pattern is carefully used to optimize the outputs to be proportional to $\cos\phi$ and $\sin\phi$, which are bounded values, i.e., not limited by dynamic range of the system electronics.

One technique for phase recovery requires digitizing the two quadrature outputs and $\tan\phi$ is computed by software, cancelling any common-mode noise or fringe contrast fluctuation. The computer next calculates the arctangent of the data yielding the phase ϕ directly, having a dynamic range only limited by the overflow capability of the computer. The optical path length, nL, is calculated

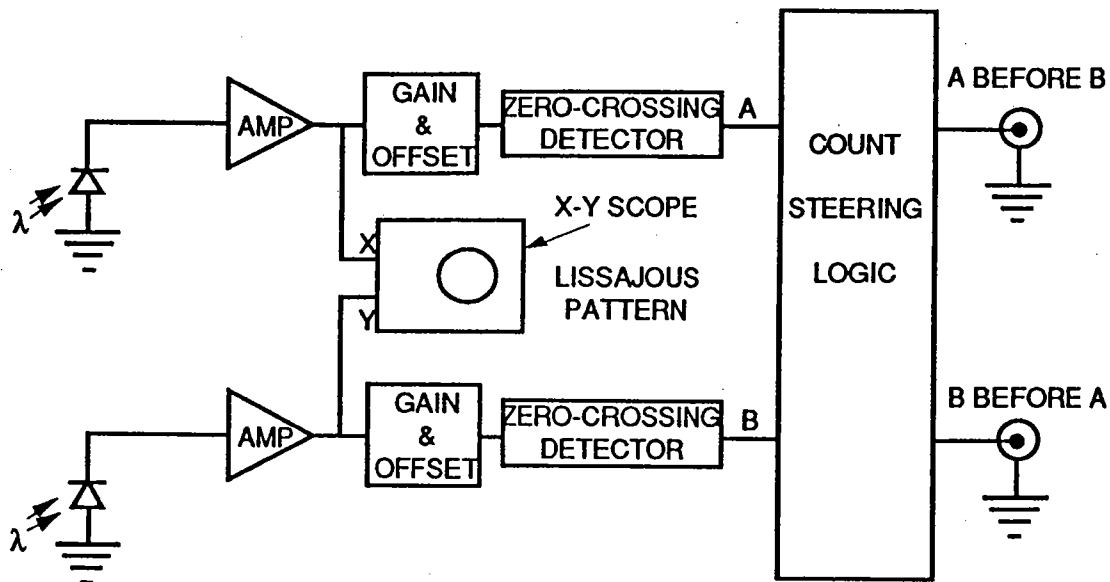$$nL = \frac{\phi\lambda}{2\pi} + (nL)_0 \tag{12}$$

Figure 5. Electronic block diagram.

This approach gives sub-fringe resolution at moderate fringe shift rates in an open-loop fashion. At higher speeds, A/D converter speed begins to limit operation.

An alternate approach for open-loop demodulation will be used, which is much simpler and requires no D/A conversion. The quadrature signals are fed to a pair of zero-crossing detectors to get digital signals: a pair of square waves offset by roughly 90 degrees. These two signals can be applied to a fast up/down counter to get the absolute count of fringes that sweep by the detectors. Each count registered by the electronics would correspond to a 2π phase shift, and corresponds to $\Delta(nL) = \lambda$.

This has the disadvantage of not being able to resolve sub-fringe shifts but has the advantages of insensitivity to offsets, gain mismatch, and nonlinearities in the quadrature signals. This method has been used in ring laser gyroscopes for years to obtain passive, bidirectional readout [8]. As this yields rate-integrated information, no differencing operation will be necessary. Both signal processing schemes will yield absolute, bidirectional, wide dynamic range data from SQD-based sensors.

EXPERIMENT

To demonstrate this approach, a single-axis device was designed, built, and tested. An aluminum cantilever 762×76×12.5 mm was fabricated, onto which six passes of optical fiber up and down the length of the cantilever were epoxied. A second

piece of 1.3-μm single-mode fiber was attached onto the bottom of the bar in a similar manner. One end of the the cantilever was affixed on a granite table; a mirror was attached to the bar's free end to permit an autocollimator to measure the deflection angle.

632.8-nm wavelength light was launched into the fibers with a helium-neon laser. At the other end, the optical fiber pair was positioned to generate the fringe pattern that was observed by a TV camera with the lens removed, located at l=12 cm from the fiber endfaces. The fringe displacement was observed on the face of the CRT. Since the fibers were simply laid side by side, the core separation d = 125 μm. This results in a fringe spacing estimate of Λ = 0.6 mm. Using a split-field photodetector, (e.g., EG&G model UV-140-2 has a gap of 100 μm) Λ = 400 μm (or some sub-multiple).

A number of trials were performed by applying different bending moments to the cantilever to verify that the sensing of alignment was independent of shape. The angle of the free end was measured with an autocollimator in all cases. A differential micrometer was mounted at different positions on the granite table and was used to displace the cantilever. Test 1 was performed by applying a force with the differential micrometer located 743 mm from the edge of the clamped end. The data shown in Figure 6 are taken every 10 fringes, for a total of 340 fringes. This corresponded to a total displacement of approximately 1 mm and an angle of about 7.5 arcminutes.

The displacement of the cantilever at the micrometer can be converted to an angle at the end by beam theory [9]. This relationship is shown in Figure 7. Notice the excellent correlation between measured angle and expected angle. The measured scale factor is calculated by dividing the angle as measured by the autocollimator by the number of fringes. This is shown in Figure 8. The average scale factor is 1.254 arcsec per fringe.

In Test 2 the micrometer was moved away from the beam's free end; applying the force at 508 mm from the fixed end gives the cantilever a different mode shape. These data are shown in Figure 9. The average scale factor measured for this shape is 1.235 arcsec per fringe.

To generate a more radical mode shape for Test 3, the cantilever's free end was constrained and the force was applied at 495 mm. In addition, to test for hysteresis in the measurement, data were taken as the force was increasing and as it was decreasing. These results are shown in Figures 10 and 11. No hysteresis was detected and the average scale factor was measured to be 1.131 arcsec per fringe.
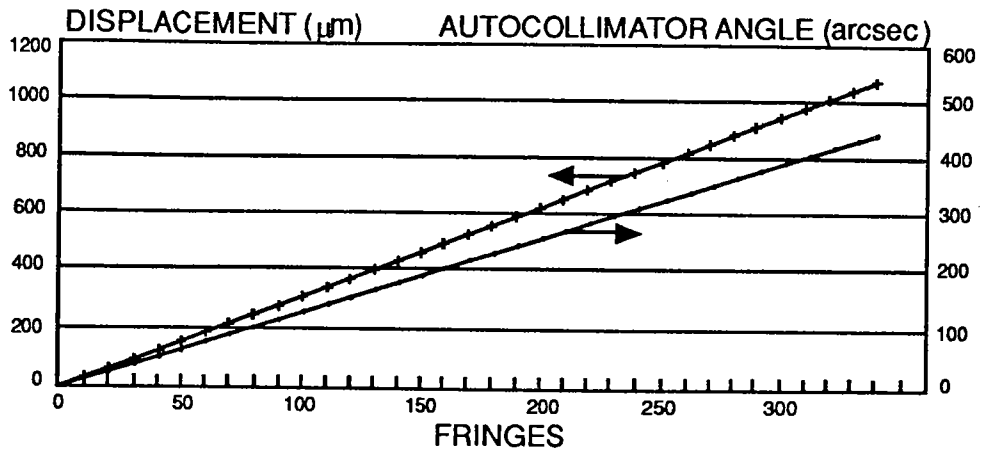
Solid-State Optical Materials

Figure 6. Measured displacement, angle and fringe count for Test 1.

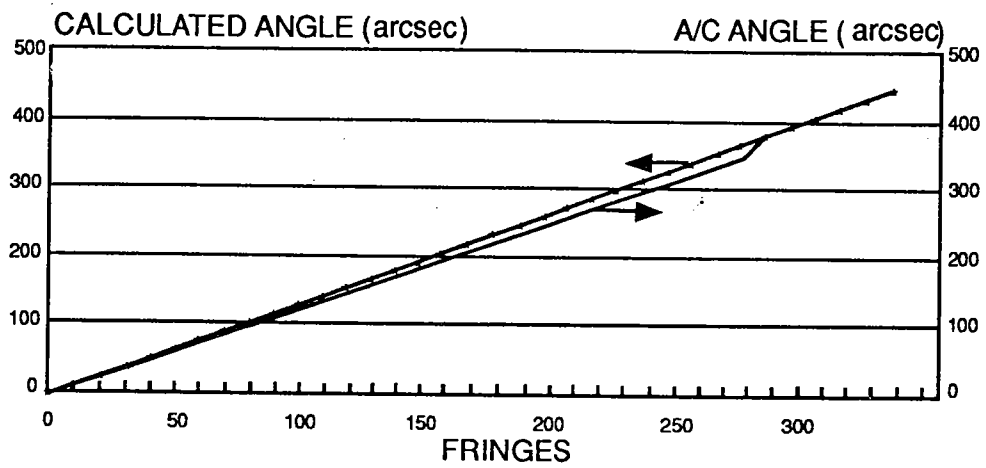Figure 7. Angular beam deflection in Test 1.

Figure 8. Scale factor data for Test 1.
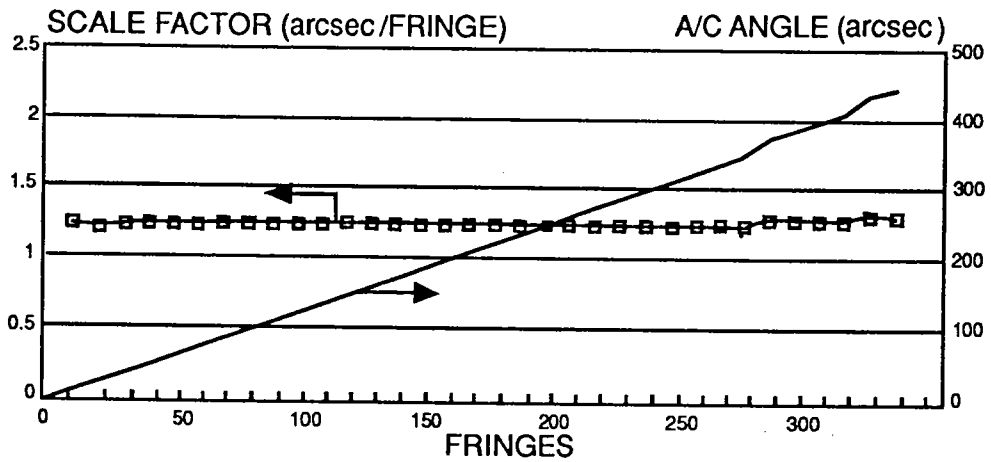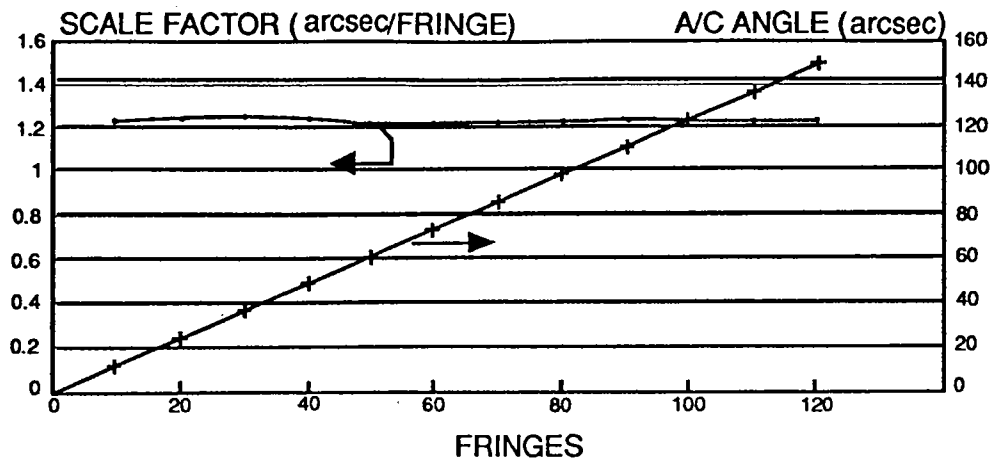
Solid-State Optical Materials   619

SCALE FACTOR (arcsec/FRINGE)   A/C ANGLE (arcsec)

Figure 9. Test 2 data.

SCALE FACTOR (arcsec/FRINGE)   A/C ANGLE (arcsec)

Figure 10. Test 3 data.

A/C ANGLE (DECREASING)   A/C ANGLE (INCREASING)
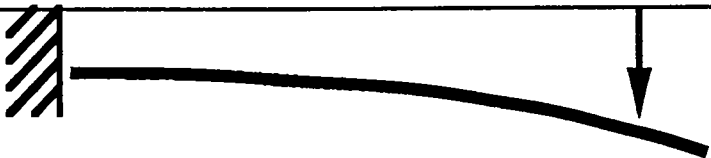(arcsec)   (arcsec)
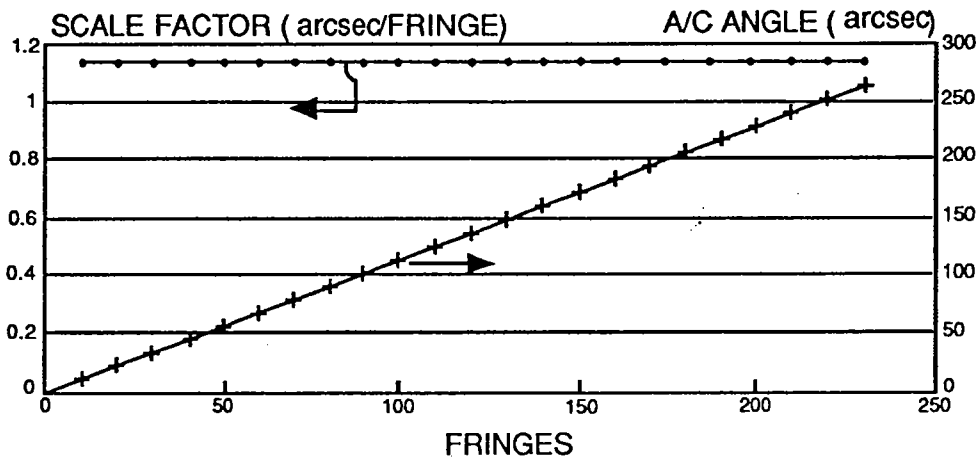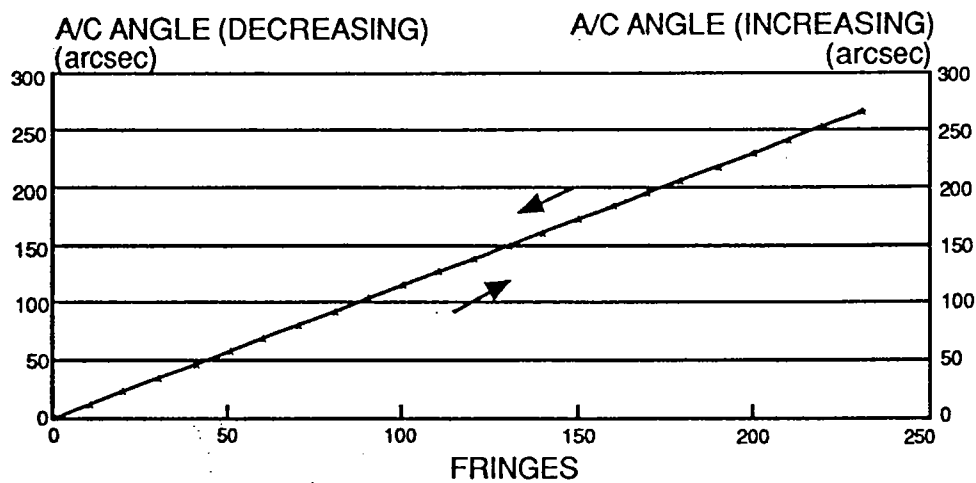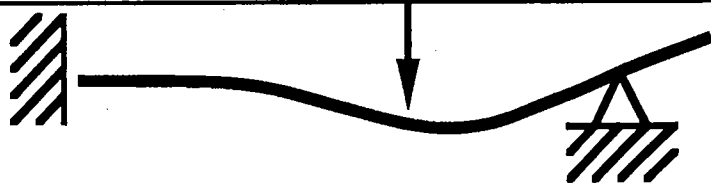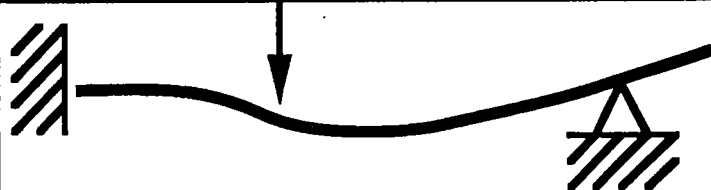
Figure 11. Test 3 data showing no hysteresis.

TASK	CONFIGURATION BENDING MODE	SCALE FACTOR
TEST 1 F @ 743 mm		1.254 arcsec/fringe
TEST 2 F @ 508 mm		1.235 arcsec/fringe
TEST 3 F @ 495 mm + FULCRUM		1.131 arcsec/fringe
TEST 4 F @ 235 mm + FULCRUM		1.116 arcsec/fringe
	AVERAGE SCALE FACTOR	1.184 arcsec/fringe

In Test 4 the micrometer was located at 235 mm while the beam end was again constrained. The results are shown in Figure 12. Again, no signs of hysteresis were seen. The average scale factor was measured to be 1.116. The mean measured scale factor for all tests is 1.184 arcsec per fringe. All scale factors deviate by less than 6 percent of this value. This shows that, to first order, the measurement is independent of the beam's shape.

The theoretical scale factor F is given by [10]:

$$F \equiv \frac{\phi}{\epsilon} = \frac{\lambda_o}{2\pi N D n \{1 - 0.5[\rho_{12} - \nu(\rho_{11} + \rho_{12})]\}} \tag{13}$$

Solid-State Optical Materials 621

where

λ_o	= 0.633 mm	vacuum wavelength of illumination
N	= 6	number of fibers on one side
D	= 0.5 inch	thickness of cantilever
n	= 1.447	unstressed index of refraction of fiber
ν	= 0.17	Poisson's ratio of fiber
ρ_{11}	= 0.121	photoelastic constant
ρ_{12}	= 0.270	photoelastic constant

For values of the tests (shown above), this theoretical scale factor is 1.5043 arcsec per fringe. In other words, the experimental scale factor indicates that the configuration is 27 percent more sensitive than is expected. In the expression above, the term in the inner brackets is due to the photoelastic effect, which relates the change of index of refraction as caused by strain in the fiber. The photoelastic effects are measured in unbounded fibers. If these photoelastic effects are ignored, then the theoretical scale factor is calculated to be 1.1838 arcsec per fringe, in remarkable agreement with the mean scale factor as determined by the experiments. This anomaly remains to be clarified; the fiber used was slightly multimoded at HeNe wavelengths, which might account for some of the discrepancy.

A first-order examination of the device's design indicates that it should be temperature independent. In fact, one is led to view the device also as independent of temperature gradients. This is certainly true of gradients along the cantilever's length. Temperature gradients across the thickness could cause the cantilever's deflection but the same indication would be registered by the readout of the fibers. However, this temperature gradient could effect the index of refraction differentially.

To test this view, the cantilever was heated to 143°F, and was permitted to stabilize at this temperature overnight. The heat was then removed and the temperature, autocollimator angle, and output were monitored during the cooldown, lasting 4.5 hr. A significant discrepancy of about 25 arcsec between the measured and indicated angle was seen at the beginning of the run. This is believed to be due to the onset of considerable time-varying temperature gradients. If the first 10 minutes of data are ignored, then the agreement between the indicated and measured angles improves. This is shown in Figure 13. Here the difference is about 13 arcsec, a remarkable achievement considering that this is over a temperature range of 50°F. Clearly, more investigation of temperature sensitivity is required.
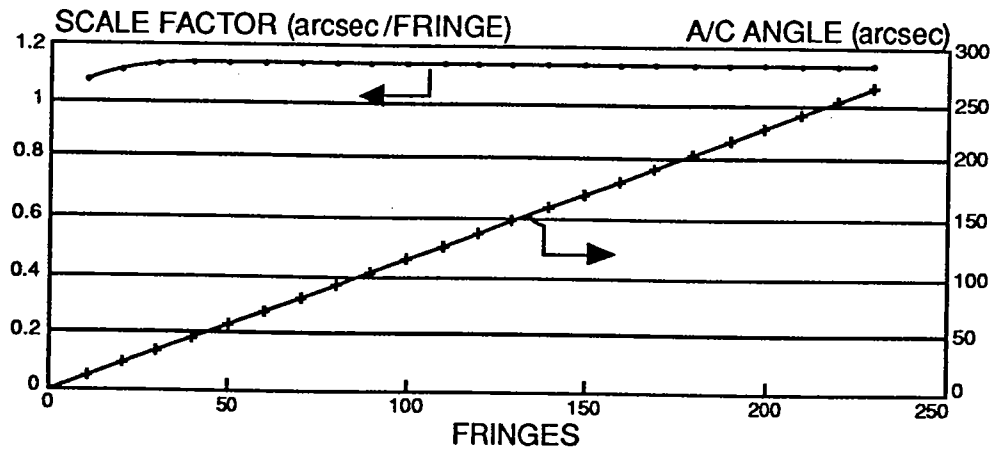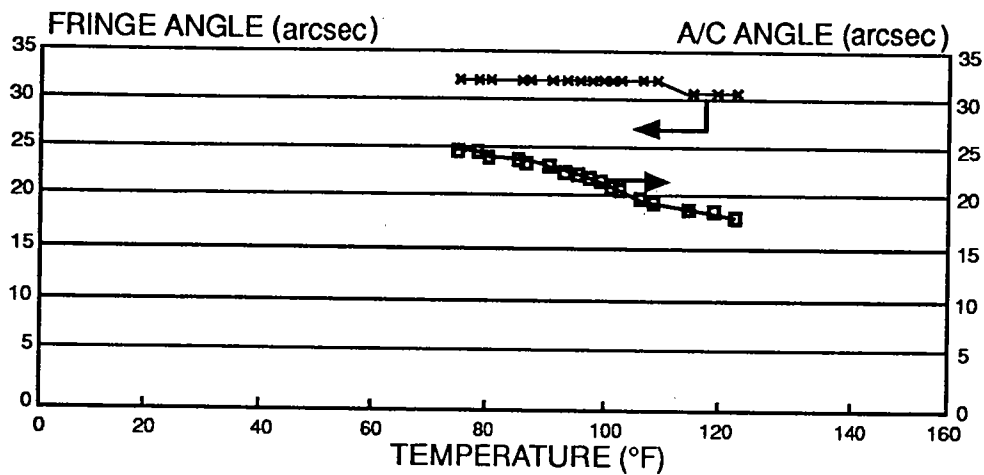
Figure 12. Test 4 data.

Figure 13. Thermal test data.

The following points summarize the results of these experiments:

(1)   Single-axis alignment determination by fiber optics has been successfully demonstrated.

(2)   Sensitivities of angular measurement of 1.2 arcsec per fringe were achieved. With reasonable fringe interpolation, 0.1-arcsec angular resolution can be shown with the test setup.

(3)   Bending mode invariance has been demonstrated.

(4)   Temperature insensitivity has been shown.

CONCLUSIONS

The following conclusions are drawn with regard to applying fiber optics to determine the shape of towed arrays.

(1)   The fiber-optic approach for this application to towed arrays is promising. All of the experimental investigations summarized above were positive. No serious concerns became evident.

(2)   Proof-of-principle of this approach was demonstrated, including adequate sensitivity, flexibility, and temperature tolerance.

(3)   More study is required for this application. For instance, the approach assumes that the diameter of the cable and array remain constant; this needs investigation. It may be difficult to attach the optical fibers to the towed array's plastic outer sheath.

REFERENCES

[1]   Hocker, G. B., "Fiber-Optic Sensing of Pressure and Temperature." *Appl. Opt.* 18(9): 1445, 1979.

[2]   Wilk, L. S., "Strain Measurement Apparatus and Method, US Patent No. 4,788,868.", 1988.

[3]   Dahlgren, R., B. Harris, J. Vanderwall, S. Krimchansky, and J. Blackburn, "Measurement of Radiation Effects on Refractive Index of PANDA High-Birefringence Fibers." *Hardened Electronics & Radiation Technology (HEART)*, 1990.

[4]   Born, M. and E. Wolf, *Principles of Optics*. MacMillan, 1964.

[5]   Nakadate, S, "Optical Fiber Sensors Using a Phase Detection of Young's Fringes." *Appl. Opt.* 27(23): 4826, 1988.

[6]   Stowe, D. and T. Hsu, "Demodulation of Interferometric Sensors Using a Fiber-Optic Passive Quadrature Demodulator." *JLWT.* 1(3): 519, 1983.

[7]   Downes, M. and K. Raine, "An Unmodulated Bi-Directional Fringe-Counting Interferometer for Measuring Displacement." *Prec. Eng.* **1**(2): 85, 1979.

[8]   Smith, R. B., Honeywell, Inc. personal communications, 1980.

[9]   Timoshenko, S. and G. H. MacCullough, *Elements of Strength of Materials*. Van Nostrand, 1950.

[10]   Bertholds, A. and R. Dandliker, "Determination of the Individual Strain-Optic Coefficients in Single-Mode Optical Fibers." *JLWT*. **6**(1): 17, 1988.